

Supporting Information

A novel broadband $\text{Ba}_3\text{Ca}_4(\text{BO}_3)_3(\text{SiO}_4)\text{Cl}:\text{Mn}^{4+}$ near-infrared phosphor with special pseudo-octahedron Mn^{4+} coordination structure

Jiutian Wang,^{a,b} Tao Tan,^{a,b} Ran Pang,^a Da Li,^a Chengyu Li,^{a,b} Su Zhang,^{a,b,*} Lihong Jiang,^{a,*} and Hongjie Zhang^a

^a State Key Laboratory of Rare Earth Resource Utilization, Changchun Institute of Applied Chemistry, Chinese Academy of Sciences, Changchun 130022, China

^b School of Applied Chemistry and Engineering, University of Science and Technology of China, Hefei 230026, China

* Corresponding authors.

E-mail addresses:

lhjiang@ciac.ac.cn (Lihong Jiang),

suzhang@ciac.ac.cn (Su Zhang).

Number of pages: 20

Number of figures: 6

Number of tables: 8

Table S1. Luminescent properties of BCBSC:0.01Mn⁴⁺ phosphor and some reported Mn⁴⁺-doped oxide phosphors in recent years.

Host	Emission range (nm)	Emission peak (nm)	FWHM (nm)	IQE (%)	Ref.
Ba ₃ Ca ₄ (BO ₃) ₃ (SiO ₄)Cl	650-1100	~765	~90	69.7	This work
Li ₃ Mg ₂ NbO ₆	600-780	~670	~50	28.6	[1]
Gd ₂ ZnTiO ₆	650-720	670, 685, 690 and 704	<50	—	[2]
Li ₂ MgTiO ₄	630-850	~676	~46	32	[3]
Na ₄ Mg(WO ₄) ₃	560-850	682	—	—	[4]
BaLaMgNbO ₆	650-800	700	~36	52	[5]
SrGdAlO ₄	650-800	709 and 725	<40	23	[6]
NaLaMgWO ₆	650-800	~700	~38	60	[7]

Table S2. Valences and effective ionic radius for related ions.⁸

Ion	Valences	CN	IR (Å)
Mn ⁴⁺	4	6	0.53
Ba ²⁺	2	11	1.57
Ca ²⁺	2	9 10	1.18 1.23
Si ⁴⁺	4	4	0.26
B ³⁺	3	3	0.01

CN: Coordination number; IR: Effective ionic radius.

Table S3. Atomic positions of BCBSC.

Atom	Site	x	y	z	Occupancy	U _{iso}
Ba1	12d	0.1476	0.2953	0.3479	1.0000	0.0125
Ca1	6c	0.4764	0.5235	-0.0054	1.0000	0.0125
Ca2	2b	0.3333	0.6667	0.6247	1.0000	0.0166
Si1	2b	0.3333	0.6667	0.2094	1.0000	0.028
B1	6c	0.8063	0.6125	0.2927	1.0000	0.0114
Cl1	2a	0	0	0.1203	1.0000	0.0195
O1	2b	0.3333	0.6667	-0.028	1.0000	0.0259
O2	12d	0.6825	0.5842	0.1971	1.0000	0.0213
O3	6c	0.4146	0.8291	0.3018	1.0000	0.0177
O4	6c	0.8355	0.6711	0.4699	1.0000	0.0410

Table S4. Bond length (Å) and O-Ca1-O bond angle (°) of BCBSC and BCBSC:0.1Mn⁴⁺.

BCBSC				BCBSC:0.1Mn ⁴⁺			
Bond length		Bond angle		Bond length		Bond angle	
Ba1-Cl1	3.15198(10)	O1-Ca1-O2	126.480(1)	Ba1-Cl1	3.15284(9)	O1-Ca1-O2	126.481(0)
Ba1-Cl1	3.31221(10)	O1-Ca1-O2	76.441(0)	Ba1-Cl1	3.31308(9)	O1-Ca1-O2	76.441(0)
Ba1-O2	2.87748(9)	O1-Ca1-O2	126.509(1)	Ba1-O2	2.87812(8)	O1-Ca1-O2	126.510(0)
Ba1-O2	2.95102(10)	O1-Ca1-O2	76.431(0)	Ba1-O2	2.95185(10)	O1-Ca1-O2	76.431(0)
Ba1-O2	2.95202(10)	O1-Ca1-O3	143.803(2)	Ba1-O2	2.95286(10)	O1-Ca1-O3	143.807(2)
Ba1-O2	2.87704(9)	O1-Ca1-O3	64.446(2)	Ba1-O2	2.87768(8)	O1-Ca1-O3	64.443(1)
Ba1-O3	3.01498(12)	O2-Ca1-O2	154.625(0)	Ba1-O3	3.01587(11)	O2-Ca1-O2	154.625(0)
Ba1-O3	3.01438(12)	O2-Ca1-O2	73.147(2)	Ba1-O3	3.01527(11)	O2-Ca1-O2	73.150(1)
Ba1-O4	3.03131(11)	O2-Ca1-O2	103.128(2)	Ba1-O4	3.03219(10)	O2-Ca1-O2	103.124(2)
Ba1-O4	2.58928(11)	O2-Ca1-O3	80.706(2)	Ba1-O4	2.58977(10)	O2-Ca1-O3	80.702(2)
Ba1-O4	3.02953(11)	O2-Ca1-O3	76.686(3)	Ba1-O4	3.03041(10)	O2-Ca1-O3	76.691(2)
Ca1-O1	2.66661(11)	O2-Ca1-O2	103.165(2)	Ca1-O1	2.66740(10)	O2-Ca1-O2	103.160(2)
Ca1-O2	2.40386(7)	O2-Ca1-O2	69.129(3)	Ca1-O2	2.40323(7)	O2-Ca1-O2	69.135(3)
Ca1-O2	2.52421(3)	O2-Ca1-O3	73.937(2)	Ca1-O2	2.52339(8)	O2-Ca1-O3	73.941(2)
Ca1-O2	2.40331(3)	O2-Ca1-O3	127.667(2)	Ca1-O2	2.40259(7)	O2-Ca1-O3	127.663(2)
Ca1-O2	2.52458(7)	O2-Ca1-O2	154.628(0)	Ca1-O2	2.52400(8)	O2-Ca1-O2	154.628(0)
Ca1-O3	2.41448(3)	O2-Ca1-O3	80.735(2)	Ca1-O3	2.41409(7)	O2-Ca1-O3	80.730(2)
Ca1-O3	2.38563(4)	O2-Ca1-O3	76.682(3)	Ca1-O3	2.38512(8)	O2-Ca1-O3	76.687(2)
Ca1-O4	2.93457(12)	O2-Ca1-O3	73.911(2)	Ca1-O4	2.93545(4)	O2-Ca1-O3	73.915(2)
Ca1-O4	2.93629(4)	O2-Ca1-O3	127.656(2)	Ca1-O4	2.93728(11)	O2-Ca1-O3	127.652(2)
Ca2-O1	2.36160(10)	O3-Ca1-O3	151.751(0)	Ca2-O1	2.36205(9)	O3-Ca1-O3	151.751(0)
Ca2-O2	2.65815(10)			Ca2-O2	2.65893(9)		
Ca2-O2	2.65920(10)			Ca2-O2	2.65998(9)		
Ca2-O2	2.65873(10)			Ca2-O2	2.65951(9)		
Ca2-O2	2.65815(10)			Ca2-O2	2.65893(9)		
Ca2-O2	2.65873(10)			Ca2-O2	2.65951(9)		
Ca2-O2	2.65920(10)			Ca2-O2	2.65998(9)		
Ca2-O3	2.66484(9)			Ca2-O3	2.66544(8)		
Ca2-O3	2.66484(9)			Ca2-O3	2.66544(8)		
Ca2-O3	2.66537(9)			Ca2-O3	2.66597(8)		
Si1-O1	1.61429(7)			Si1-O1	1.61460(6)		
Si1-O3	1.63558(6)			Si1-O3	1.63604(5)		
Si1-O3	1.63558(6)			Si1-O3	1.63604(5)		
Si1-O3	1.63644(6)			Si1-O3	1.63690(5)		
B1-O2	1.37037(4)			B1-O2	1.37074(4)		
B1-O2	1.36945(4)			B1-O2	1.36982(4)		
B1-O4	1.32242(5)			B1-O4	1.32269(4)		

Table S5. Polyhedral distortion indices in different Mn⁴⁺-activated hosts.

Host	Space group	$\langle \lambda \rangle$	σ^2	Ref.
Ba ₃ Ca ₄ (BO ₃) ₃ (SiO ₄)Cl	Hexagonal <i>P6₃mc</i>	1.12	449.48	This work
Na ₂ WO ₂ F ₄	Orthorhombic <i>C_{2v}-pbcn</i>	1.02485	78.5316	[9]
Rb ₂ GeF ₆	Hexagonal <i>C₃-p6₃mc</i>	1.00340	35.3698	[10]
K ₂ SiF ₆	Cubic <i>O_h-Fm₃m</i>	1.00000	0.0000	[11]
La ₄ Ti ₃ O ₁₂	Rhombohedral <i>C₃-R</i>	1.00370	56.9296	[12]

Table S6. Spectroscopic parameters and calculated β_1 values of Mn⁴⁺ ions in various hosts.

Host	Dq (cm ⁻¹)	B (cm ⁻¹)	C (cm ⁻¹)	β_1	E(² E _g) (cm ⁻¹)	Ref.
3.5MgO·0.5MgF ₂ ·GeO ₂	2381	700	3416	0.997	15,151	[13]
BaSiF ₆	2128	568	3879	1.025	16,048	[14]
Na ₂ SiF ₆	1970	775	3490	1.051	16,210	[15]
K ₂ GeF ₆	2123	590	3831	1.025	16,050	[16]
K ₂ SiF ₆	2030	770	3470	1.044	15,873	[17]
LiAl ₅ O ₈	2014	725	2900	0.92	13,977	[18]
NaLaMgTeO ₆	2008	790	2949	0.966	14,676	[19]
LiGa ₅ O ₈	—	653	3289	0.949	14,724	[20]
SrTiO ₃	1818	719	2839	0.905	13,827	[21]
Ba ₂ LaNbO ₆	1780	670	3290	0.958	14,679	[22,23]
LaAlO ₃	2123	700	2941	0.912	14,045	[24]
Zn ₂ TiO ₄	2156	691	3198	0.952	14,815	[25]
Mg ₂ TiO ₄	2096	700	3348	0.985	15,267	[26]
CaZrO ₃	1850	754	3173	0.983	15,054	[27]
Sr ₄ Al ₁₄ O ₂₅	2222	790	3192	1.007	15,337	[28]
CaAl ₁₂ O ₁₉	2146	750	3245	0.993	15,243	[29]
SrMgAl ₁₀ O ₁₇	2237	791	3084	0.989	15,152	[30]
Y ₂ Sn ₂ O ₇	2100	700	3515	1.016	15,563	[31]
Y ₃ Ga ₅ O ₁₂	1922	699	3197	0.957	14,859	[25]
Mg ₁₄ Ge ₅ O ₂₄	2375	709	3263	0.974	15,175	[25]
YAl ₃ (BO ₃) ₄	1890	755	3015	0.956	14,620	[32]
Li ₂ MgTiO ₄	2101	724	3122	0.957	14,793	[33]
SrGe ₄ O ₉	2362	832	3024	1.004	15,267	[25]
Gd ₂ ZnTiO ₆	2041	794	2783	0.924	14,205	[34]
Mg ₃ Ga ₂ SnO ₈	2033	847	2846	0.99	14,706	[35]
BaLaMgNbO ₆	1923	736	2944	0.93	14,286	[36]
Ba ₃ Ca ₄ (BO ₃) ₃ (SiO ₄)Cl	2128	567	2958	0.843	13,228	This work

Table S7. The device performance of BCBSC:0.01Mn⁴⁺ NIR pc-LED excited by 365 nm n-UV chip.

Current (mA)	Voltage (V)	Input power (mW)	Output power (mW)
10	3.192	31.92	0.6813
20	3.234	64.36	1.665
30	3.261	97.51	2.667
40	3.282	130.9	3.604
50	3.3	164.6	4.481
60	3.314	198.5	5.253
70	3.327	232.5	5.911
80	3.339	266.7	6.531
90	3.349	301.1	6.998
100	3.359	335.5	7.408
110	3.369	370.3	7.818
120	3.377	404.9	8.018
130	3.385	439.8	8.203

Table S8. The device performance of BCBSC:0.01Mn⁴⁺ NIR pc-LED excited by 460 nm blue chip.

Current (mA)	Voltage (V)	Input power (mW)	Output power (mW)
10	2.623	26.23	1.801
20	2.667	53.07	3.391
30	2.702	80.78	4.764
40	2.732	109	5.904
50	2.76	137.7	6.827
60	2.786	166.9	7.624
70	2.811	196.5	8.215
80	2.836	226.6	8.706
90	2.859	257	9.021
100	2.881	287.8	9.236
110	2.904	319.1	9.389
120	2.925	350.7	9.419
130	2.947	382.8	9.429

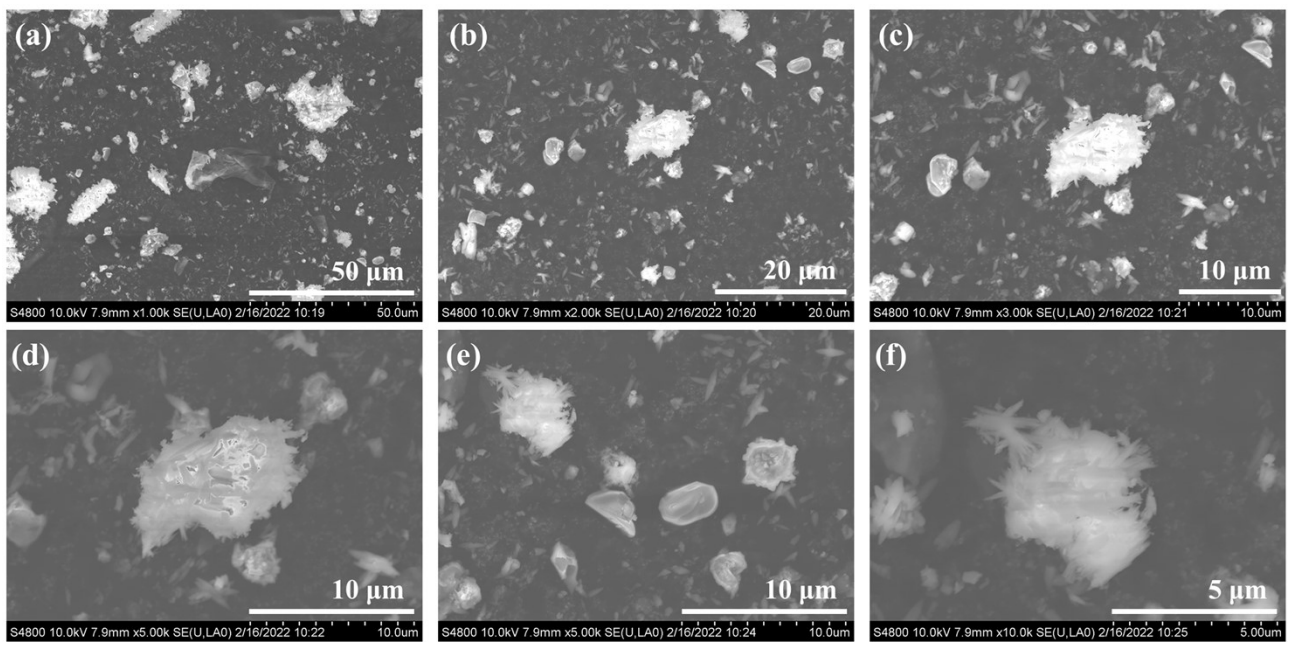


Fig. S1. SEM images of BCBSC:0.1Mn⁴⁺ phosphor in different magnification of (a) ×1000, (b) ×2000, (c) ×3000, (d) ×5000, (e) ×5000, and (f) ×10000.

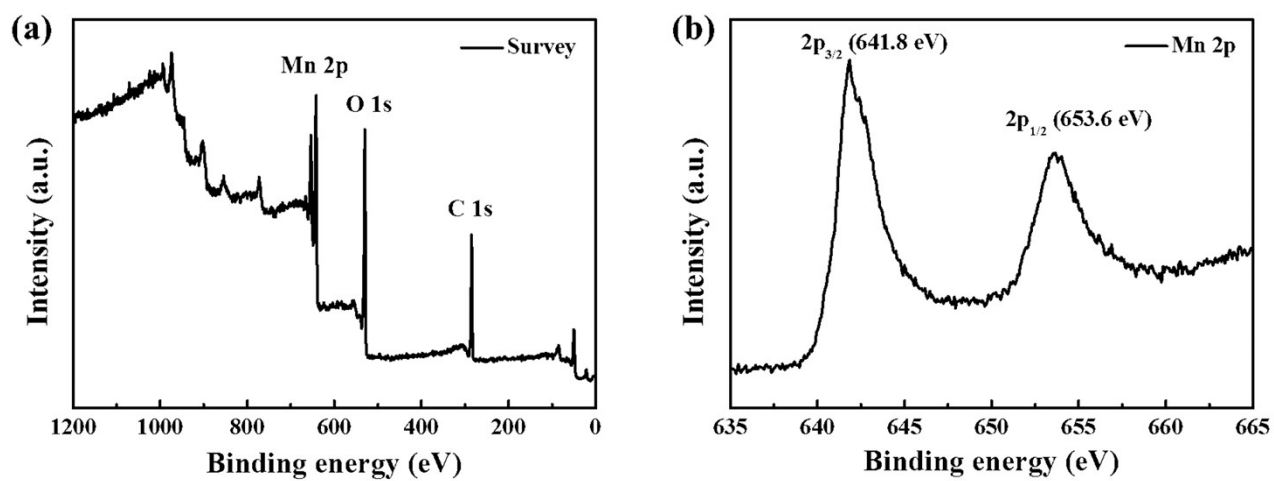


Fig. S2. (a) XPS survey spectrum of MnO_2 standard sample. (b) the magnified Mn 2p spectrum.

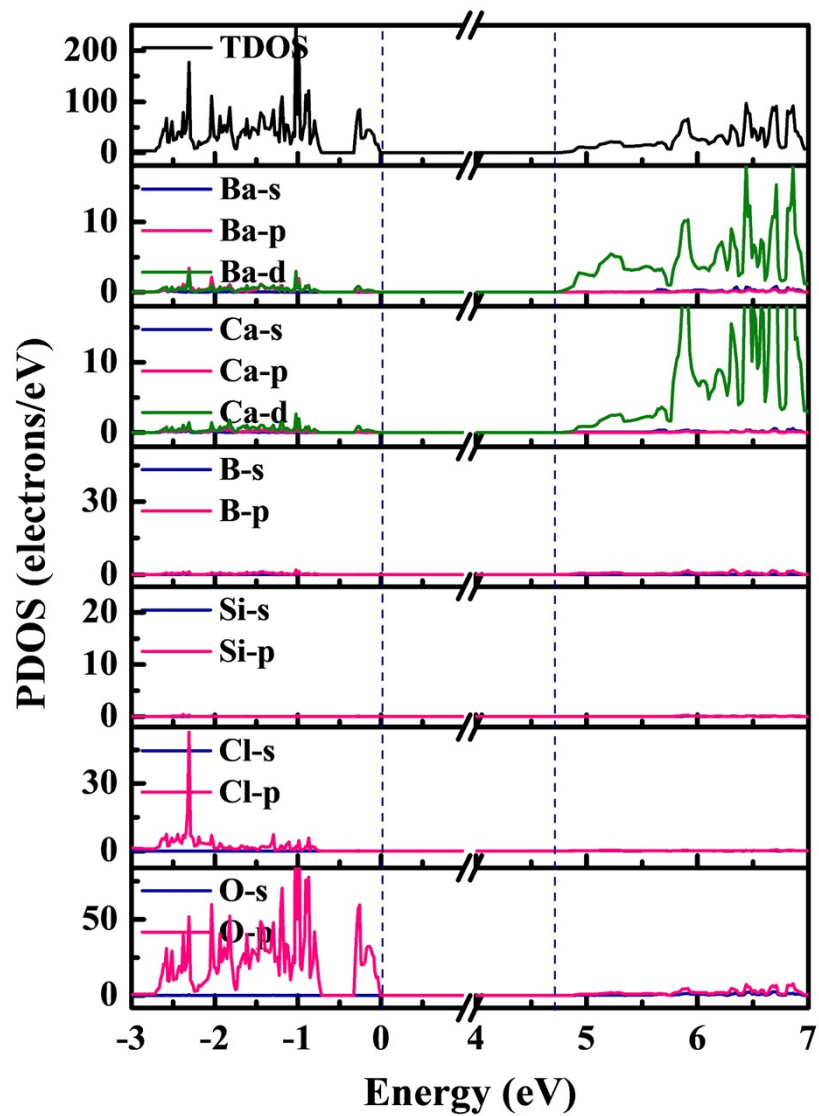


Fig. S3. The local magnification PDOS of BCBSC.

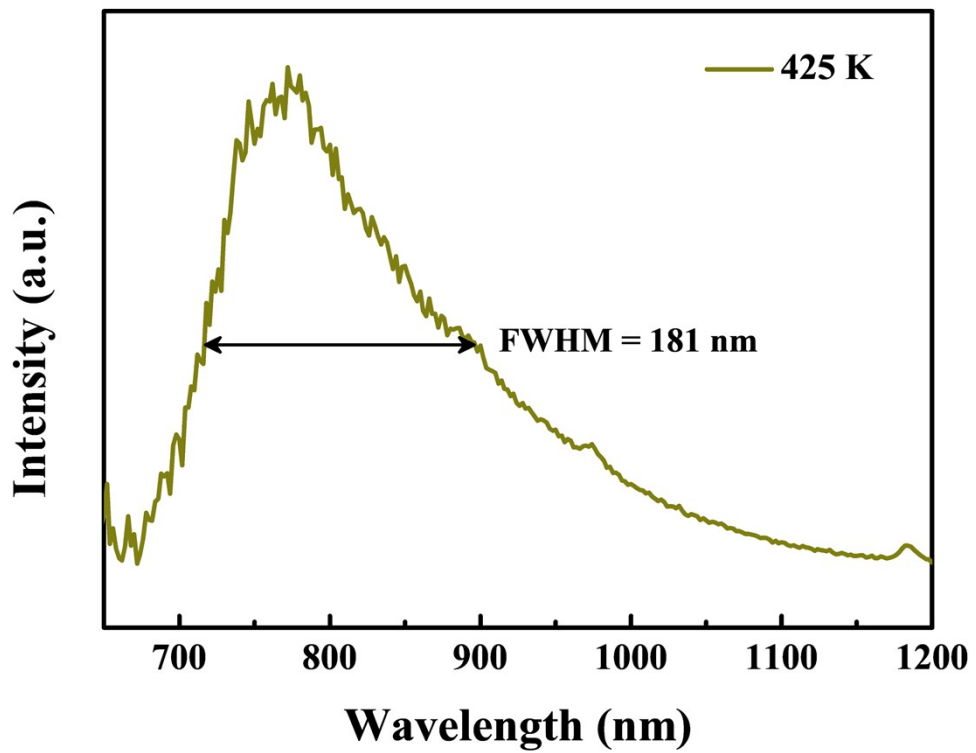


Fig. S4. The PL spectrum of the BCBSC:0.1Mn⁴⁺ phosphor measured at 425 K.

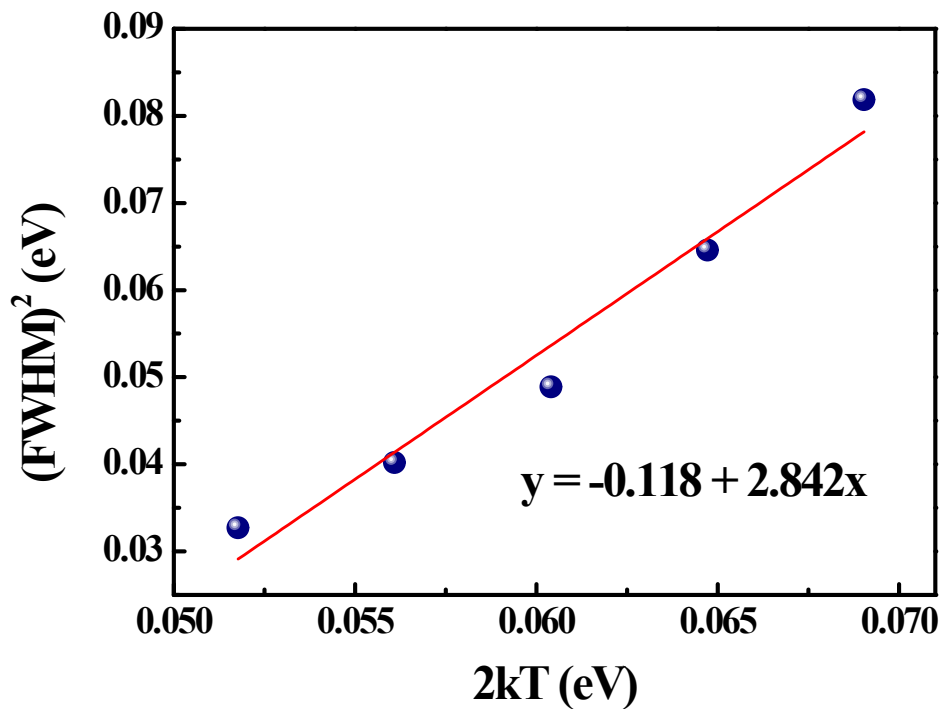


Fig. S5. Fitting results of square of full width at half maximum (FWHM^2) as a function of $2kT$.

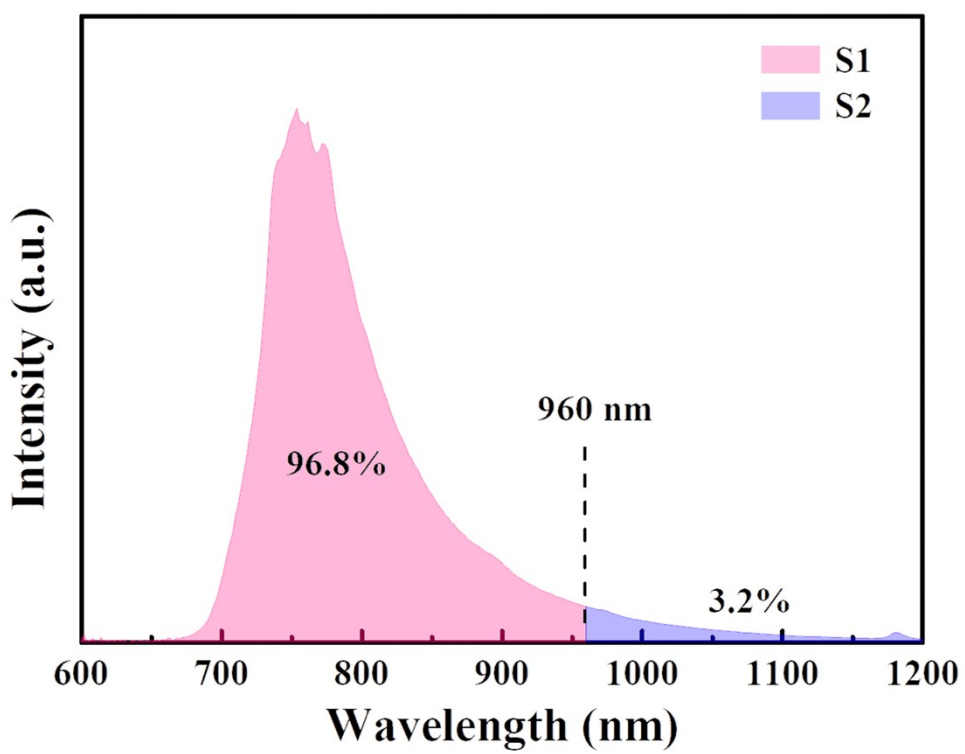


Fig. S6. The integral area of the PL spectrum of the BCBSC:0.1Mn⁴⁺ phosphor in the range of 600–960 nm and 960–1200 nm, respectively.

Supplementary Note

Computational Detail

Based on density functional theory (DFT), the band structure and electronic structure were calculated by Vienna ab initio simulation package (VASP) codes. The exchange correlation potential was approximated by generalized gradient approximation (GGA) using the Perdew–Burke–Ernzerhof (PBE) formulation. We used the projected augmented wave (PAW) potentials to describe the ionic cores. The plane wave basis set with a kinetic energy cutoff of 450 eV and we used $2\times2\times2$ for the Monkhorst-Pack k-point for sampling the Brillouin zone during the whole computations. Partial occupancies of the Kohn–Sham orbitals were allowed using the Gaussian smearing method and a width of 0.05 eV. The electronic energy was considered to be self-consistent when the energy change was less than 10^{-5} eV. The geometric optimization was considered convergent when the force change was less than 0.02 eV/Å.

References

1. R. Cao, Z. Shi, G. Quan, Z. Luo, P. Tang, H. Ao and X. Yu, $\text{Li}_3\text{Mg}_2\text{NbO}_6:\text{Mn}^{4+}$ red phosphor for light-emitting diode: Synthesis and luminescence properties, *Opt. Mater.*, 2016, **57**, 212-216.
2. H. G. Xiang, Chongfeng Far red and near infrared double-wavelength emitting phosphor $\text{Gd}_2\text{ZnTiO}_6:\text{Mn}^{4+}, \text{Yb}^{3+}$ for plant cultivation LEDs, *Dyes Pigments*, 2018, **154**.
3. Y. H. Jin, Yihua; Wu, Haoyi; Duan, He; Chen, Li; Fu, Yinrong; Ju, Guifang; Mu, Zhongfei; He, Miao, A deep red phosphor $\text{Li}_2\text{MgTiO}_4:\text{Mn}^{4+}$ exhibiting abnormal emission: Potential application as color converter for warm w-LEDs, *Chem. Eng. J.*, 2016, **288**, 596-607.
4. D. K. Amarasinghe and F. A. Rabuffetti, Bandshift Luminescence Thermometry Using $\text{Mn}^{4+}:\text{Na}_4\text{Mg}(\text{WO}_4)_3$ Phosphors, *Chem. Mater.*, 2019, **31**.
5. W. Li, L. Sun, B. Devakumar, N. Ma and X. Huang, Synthesis, crystal structure and photoluminescence properties of novel far-red-emitting $\text{SrLaZnSbO}_6:\text{Mn}^{4+}$ double-perovskite phosphors for plant cultivation LEDs, *J. Photoch. Photobio. A*, 2021, **410**, 113166.
6. Q. W. Sun, Shaoying; Devakumar, Balaji; Li, Bin; Huang, Xiaoyong Novel far-red-emitting $\text{SrGdAlO}_4:\text{Mn}^{4+}$ phosphors with excellent responsiveness to phytochrome PFR for plant growth lighting, *RSC Adv.*, 2018, **8**, 39307-39313.
7. X. L. Huang, Jia; Li, Bin; Sun, Liangling; Lin, Jun High-efficiency and thermally stable far-red-emitting $\text{NaLaMgWO}_6:\text{Mn}^{4+}$ phosphorsfor indoor plant growth light-emitting diodes, *Opt. lett.*, 2018, **43**.
8. R. D. Shannon, Revised Effective Ionic Radii and Systematic Studies of Interatomic Distances in Halides and Chalcogenides, *Acta Crystallogr. Sect.*, 1976, **32**, 751-767.
9. T. L. Hu, Hang; Cheng, Yao; Huang, Qingming; Xu, Ju; Gao, Yan; Wang, Jiaomei; Wang, Yuansheng A highly-distorted octahedron with a $\text{C}2\text{v}$ group symmetry inducing an ultra-intense zero phonon line in Mn^{4+} -activated oxyfluoride $\text{Na}_2\text{WO}_2\text{F}_4$, *J. Mater. Chem. C*, 2017, **5**, 10524-10532.
10. S. S. N. T. A. Sadao, Synthesis and properties of $\text{Rb}_2\text{GeF}_6:\text{Mn}^{4+}$ red-emitting phosphors, *Jpn. J. of Appl. Phys.*, 2018, **57**, 22601.
11. A. G. Paulusz, Efficient Mn(IV) Emission in Fluorine Coordination, *J. Electrochem. Soc.*,

- 1973, **120**, 942-947.
12. H. Ji, J. Ueda, M. G. Brik, M.-H. Du, D. Chen and S. Tanabe, Intense deep-red zero phonon line emission of Mn⁴⁺ in double perovskite La₄Ti₃O₁₂, *Phys. Chem. Chem. Phys.*, 2019, **21**, 25108-25117.
 13. S. Okamoto and H. Yamamoto, Luminescent-Efficiency Improvement by Alkaline-Earth Fluorides Partially Replacing MgO in 3.5MgO·0.5MgF₂·GeO₂:Mn⁴⁺ Deep-Red Phosphors for Light Emitting Diodes, *J. Electrochem. Soc.*, 2010, **157**, J59.
 14. D. Sekiguchi, J.-i. Nara and S. Adachi, Photoluminescence and Raman scattering spectroscopies of BaSiF₆:Mn⁴⁺ red phosphor, *J. Appl. Phys.*, 2013, **113**, 183516.
 15. Y. K. Xu and S. Adachi, Properties of Na₂SiF₆:Mn⁴⁺ and Na₂GeF₆:Mn⁴⁺ red phosphors synthesized by wet chemical etching, *J. Appl. Phys.*, 2009, **105**, 013525.
 16. L.-L. Wei, C. C. Lin, M.-H. Fang, M. G. Brik, S.-F. Hu, H. Jiao and R.-S. Liu, A low-temperature co-precipitation approach to synthesize fluoride phosphors K₂MF₆:Mn⁴⁺ (M = Ge, Si) for white LED applications, *J. Mater. Chem. C*, 2015, **3**, 1655-1660.
 17. T. Takahashi and S. Adachi, Mn⁴⁺-Activated Red Photoluminescence in K₂SiF₆ Phosphor, *J. Electrochem. Soc.*, 2008, **155**, E183.
 18. W. M. Yen, *Phosphor handbook*, CRC Press, 2006.
 19. A. M. Srivastava, M. G. Brik, S. J. Camardello, H. A. Comanzo and F. Garcia-Santamaria, Optical Spectroscopy and Crystal Field Studies of the Mn⁴⁺ Ion (3d³) in the Double Perovskite NaLaMgTeO₆ Z. *Naturforsch. B*, 2014, **69**, 141-149.
 20. M. G. Ciresan, M. L. Stanciu and N. M. Avram, Calculation of Optical and Spin-Hamiltonian Parameters for Mn⁴⁺ Doped in LiGa₅O₈, *Acta Phys. Pol.*, 2009, **116**, 547.
 21. Z. Bryknar, V. Trepakov, Z. Potůček and L. Jastrabík, Luminescence spectra of SrTiO₃:Mn⁴⁺, *J. Lumin.*, 2000, **87**, 605-607.
 22. P. A. Tanner and Z. Pan, Luminescence Properties of Lanthanide and Transition Metal Ion-Doped Ba₂LaNbO₆: Detection of MnO₆⁸⁻ and CrO₆⁹⁻ Clusters, *Inorg. Chem.*, 2009, **48**, 11142-11146.
 23. A. M. Srivastava and M. G. Brik, Ab initio and crystal field studies of the Mn⁴⁺-doped Ba₂LaNbO₆ double-perovskite, *J. Lumin.*, 2012, **132**, 579-584.
 24. M. G. Brik and A. M. Srivastava, On the Optical Properties of the Mn⁴⁺ Ion in Solids, *J.*

Lumin., 2013, **133**, 69-72.

25. T. M. Chen and J. T. Luo, Highly saturated red-emitting Mn (IV) activated phosphors and method of fabricating the same *U. S. Pat.*, 2010.
26. J. Stade, D. Hahn and R. Dittmann, New aspects of the luminescence of magnesiumtitanate part II: Activation with manganese, *J. Lumin.*, 1974, **8**, 318-325.
27. M. Brik and A. Srivastava, Electronic energy levels of the Mn⁴⁺ ion in the perovskite, CaZrO₃, *J. Solid State Sc.*, 2013, **2**, R148-R152.
28. M. Peng, X. Yin, P. A. Tanner, M. G. Brik and P. Li, Site Occupancy Preference, Enhancement Mechanism, and Thermal Resistance of Mn⁴⁺ Red Luminescence in Sr₄Al₁₄O₂₅: Mn⁴⁺ for Warm WLEDs, *Chem. Mater.*, 2015, **27**, 2938-2945.
29. M. G. Brik, Y. X. Pan and G. K. Liu, Spectroscopic and crystal field analysis of absorption and photoluminescence properties of red phosphor CaAl₁₂O₁₉:Mn⁴⁺ modified by MgO, *J. Alloy. Compd.*, 2011, **509**, 1452-1456.
30. L. Meng, L. Liang and Y. Wen, Deep red phosphors SrMgAl₁₀O₁₇:Mn⁴⁺, M (M = Li⁺, Na⁺, K⁺, Cl⁻) for warm white light emitting diodes, *J. Mater. Sci.-Mater. El.*, 2014, **25**, 2676-2681.
31. M. G. Brik and A. M. Srivastava, Comparative crystal field analysis of energy level schemes and nephelauxetic effect for Cr⁴⁺, Cr³⁺, and Mn⁴⁺ ions in Y₂Sn₂O₇ pyrochlore, *Opt. Mater.*, 2013, **35**, 1251-1256.
32. A. S. Aleksandrovsky, I. A. Gudim, A. S. Krylov and V. L. Temerov, Luminescence of yttrium aluminum borate single crystals doped with manganese, *Phys. Solid State*, 2007, **49**, 1695-1699.
33. Y. Jin, Y. Hu, H. Wu, H. Duan, L. Chen, Y. Fu, G. Ju, Z. Mu and M. He, A Deep Red Phosphor Li₂MgTiO₄:Mn⁴⁺ Exhibiting Abnormal Emission: Potential Application as Color Converter for Warm w-LEDs, *Chem. Eng. J.*, 2016, **288**, 596-607.
34. J. Xiang, J. Chen, N. Zhang, H. Yao and C. Guo, Far Red and Near Infrared Double-Wavelength Emitting Phosphor Gd₂ZnTiO₆: Mn⁴⁺, Yb³⁺ for Plant Cultivation LEDs, *Dyes and Pigments*, 2018, **154**, 257-262.
35. Q. Zhu, J. Huo, Y. Lin, M. Li, W. Liu, J. Gao and Q. Wang, A New Co-Substitution Strategy as a Model to Study a Rare-Earth-Free Spinel-Type Phosphor with Red Emissions

- and Its Application in Light-Emitting Diodes, *Inorg. Chem.*, 2020, **59**, 433-442.
36. Q. Sun, S. Wang, B. Devakumar, B. Li, L. Sun, J. Liang and X. Huang, Synthesis and Photoluminescence Properties of Novel Far-Red-Emitting BaLaMgNbO₆:Mn⁴⁺ Phosphors for Plant Growth LEDs, *RSC Adv.*, 2018, **8**, 28538-28545.